ÉCOLE POLYTECHNIQUE
FÉDÉRALE DE LAUSANNE

Semester Project SMT

February 2016 – Mai 2016

Multi-sensory Autonomous Docking Approach for a Self-reconfigurable Robot without Mechanical Guidance

Author:
Stephane Bussier

Supervisor:
Prof. Auke Ijspeert
Mehmet Mutlu

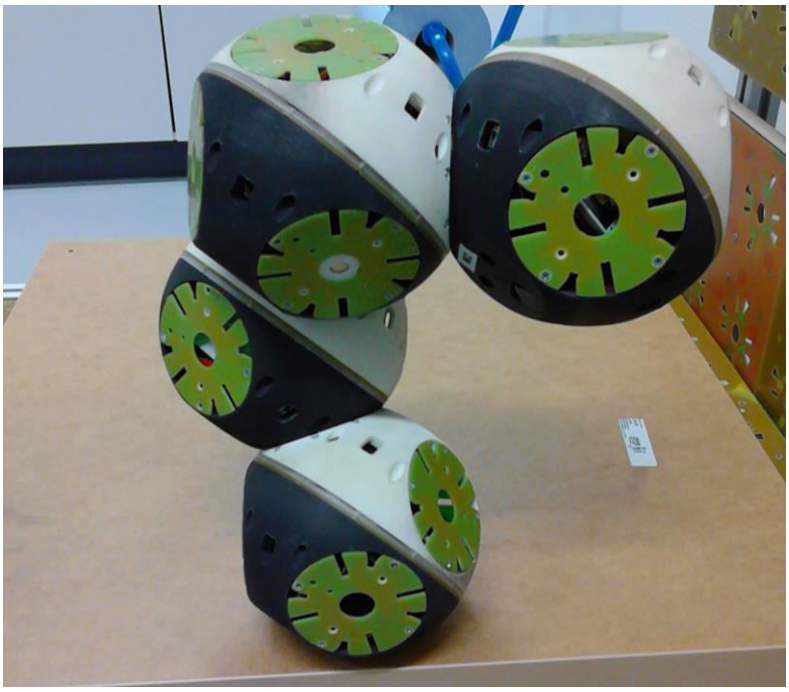

A final report submitted in partial fulfillment for the semester project conducted in the

BioRob Lab
Microtechnique Section
EPFL

Abstract

As a mean to enhance the capabilities of the roombot to undergo reconfiguration, local proximity sensors, hall sensors and infrared sensors, have been mounted on the roombot's face. With these sensors a study of the different kind of misalignment between two roombot's faces were done in this report. It demonstrates that due to the numerous symmetrical solutions, the sensors alone cannot be used to differentiate them.

Some experiments was done to characterise and choose the optimal hall sensor magnet pair and to characterise the infrared sensor. For further experimentation, the AO hall with a 4mm magnet ant the RA hall with a 3mm magnet was chosen. This two sensor magnet pairs have a range of around 1mm up to 4mm in head on direction (z) and around 1.25 up to 3mm in lateral direction (R). The infrared sensor gives operates from 0.8mm to 10mm in z and detect a $\emptyset$ (rotation around y) misalignment in a range of 2.7° to 9°. The infrared sensor mounted horizontally cannot detect a misalignment in θ (rotation around x).

After having done further testing on the roombot, the hall sensors enable the detection of a misalignment and therefore indicates if it is safe or not to activate the Active Connection Mechanism (ACM) to dock.

1 INTRODUCTION

A self-reconfigurable modular robot is one, which is able to deliberately change their own shape by rearranging the connectivity of their parts, in order to adapt to new circumstances, perform new tasks, or recover from damage. Modular robots generally consist of actuators and transmission mechanisms that are the most important and constraining aspects. They are mainly used for locomotion and in active connection mechanisms (ACM). Modular robots may consist of additional units like cameras, proximity sensors, encoders, that give some feedback in the state of the robot. On critical aspect associated with modular robot, so as it can undergo autonomous transformations between different configurations, is its ability to achieve safe docking.

Roombot is considered as a self-reconfigurable modular robot. It consist of four half shells that contains three actuators that gives a roombot module three degrees of freedom (3 DOF). Another important part is its hermaphrodite active connection mechanism where the roombot's face consists of both male and female connection features. The ACM enables the roombot to connect to other roombot's ACM or passive surfaces. A circular array of magnet, in front of the ACM, has been added in the new version of the roombot that acts as guidance during the docking process. To obtain a metamodule, two roombot's modules need to be connected to each other. This enables a 6 DOF movement due to the presence of 6 actuators in series.

1.1 MOTIVATION

The motivation of this project is to enhance roombot self-reconfigurable capabilities. This begins by enhancing the docking process between roombot modules. To ensure safe docking a good alignment between roombots is required. This is important in order not to break the ACM because if not well aligned, the grippers will not enter in a female connector and break the device. In this case sensory guidance has been chosen other mechanical guidance mostly due to the limited amount of space on the roombot and to maintain the flexibility of the reconfiguration.

1.2 GOAL OF THIS PROJECT

This project can be divided into four parts:

- A theoretical analysis and classification of the different kind misalignment that may happen during the docking process.
- How the hall and infrared sensor can be used to differentiate the different misalignments.
- Characterising the behaviour of the infrared and hall sensors given by doing some experiments. Then choosing the best proximity sensors.
- Doing further experiments on roombot hardware to evaluate docking process.

2 APPLICABLE PROXIMITY SENSORS

A proximity sensor is a sensor able to detect the presence of physical objects without physical contact. There exist different type of proximity sensors that are mostly exteroceptive sensors, i.e. they take information about the robot's environment. Inductive sensors, capacitive sensors, hall sensors, infrared sensors, ultrasound sensors are examples of proximity sensors. Table 2.1 make a comparison between proximity sensors that can be found on the market.

Table 2.1:Proximity sensors Comparison

Proximity sensors	What is being sensed	Target material	Sensor Size [mm]
Inductive (LMP91300YZR)	A change in magnetic field	Metal	2.05 x 2.67 + coils size
Capacitive (FDC2214)	Electric field	Any	4 x 4 + sensing plate size
Infrared (QRE1113GR)	Repelled infrared beam	Reflective surfaces	2.9 x 3.6
Hall effect (Drv5053)	Magnetic field	Magnetic	2.9 x 1.3 + magnet size

Due to the limited amount of space on the roombot and considering the material the roombot is made of (plastic). Choosing hall and infrared sensors is more suitable in this case. Hall sensors is not affected by non-ferromagnetic material like plastic and the chip is very compact compared to the capacitive and inductive sensors which are large considering that the sensing coils and sensing plate respectively can be large. Concerning the infrared sensor it is also more compact and the mate green face of the roombot easily reflects the infrared beam.

3 SENSORS USED FOR AUTONOMOUS DOCKING

Vision is a good method to detect the position of the two modules that will undertake docking. But as the modules approaches each other, vision feedback is not able to detect precisely the misalignment between two roombot's faces that are very close to each other. Therefore, to guide the moving roombot to align to the fixed one, close sensory feedback is required. For this purpose, four hall sensors, four magnets and two infrared sensors have been mounted on the faces of the roombot (see Figure 3.1).

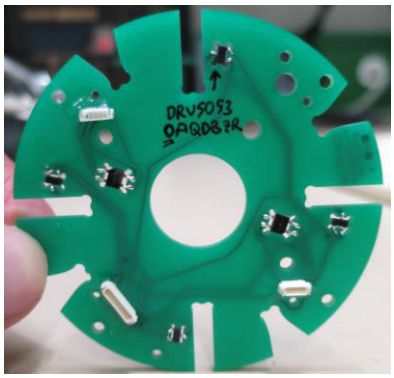

Figure 3.1: Mounted Sensors and connectors

By fusing both sensors and by knowing the commands sent to the roombot, it is possible to know in which geometrical misalignment the robot is encountering. This section will focus on how both sensors works and then in the next section focus will be put on the geometry of the detectable misalignment.

3.1 HALL SENSOR

Hall sensors use the Hall effect to detect the presence of a magnetic field. It consist of a conductor carrying current that will generate a voltage perpendicular to the current if the sensor is placed into a magnetic field, see Figure 3.2.

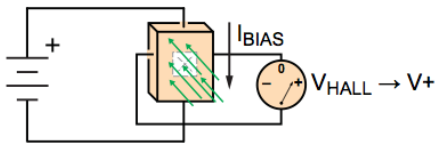

Figure 3.2: Hall effect, induced VHall, resulting from magnetic flux (green arrow) perpendicular to the bias current flow (Ref. 3)

The four magnets placed on the surfaces of the roombot are the sources of the magnetic flux density, B [T], and the four hall sensors are able to detect the changing magnetic flux density as their corresponding magnets moves towards or away from them. The hall sensors can have two modes of operations:

1. Head-on mode

In this case, the magnetic pole moves perpendicularly straight at the face of the hall sensor. It can be observed from Figure 3.3 that the magnetic flux density decreases as the magnet moves away from the hall sensor.

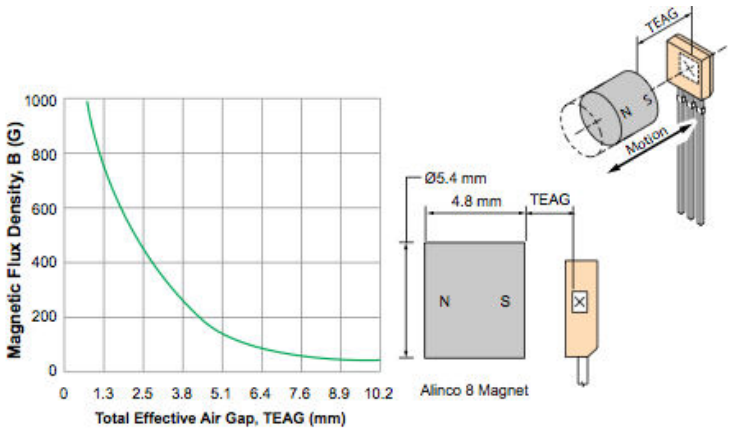

Figure 3.3: Characteristic curve of the magnetic flux against the total effective air gap. (Ref. 3)

2. Slide-by mode

In slide-by mode the magnet has a lateral motion relative to the hall sensor. The distance of motion is measured between the centreline of the magnet and the hall sensor. It can be observed from Figure 3.4 that the detection is better if the gap decreases and if the magnet does not go too far from the hall sensor. The problem of the hall sensor in this case is that, it is difficult to know the direction of motion of the magnet.

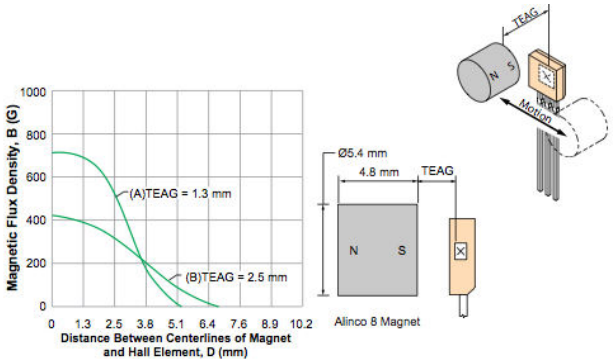

Figure 3.4: Characteristic curve of the magnetic flux obtained as the magnet moves laterally (Ref.3)

3.1.1 Characteristic of the chosen hall sensors

The four different hall sensor chosen have different negative sensitivity (-mV/T) and different saturation point.

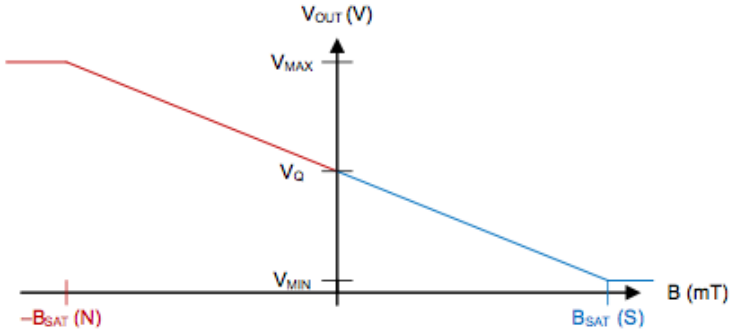

Figure 3.5:Graph of output voltage as a function of magnetic flux density, B (Ref. 8)

The quiescent voltage, V_Q is around 1V for the four hall sensors.

From Figure 3.5 the shape of the graph that linked the output voltage to the distance, z between the hall sensor and a magnet can be deduced. If a South Pole is facing the hall sensor, the magnetic flux density will decrease as z increases. Thus, the output voltage of the hall sensor will increase non-linearly (see Figure 3.6).

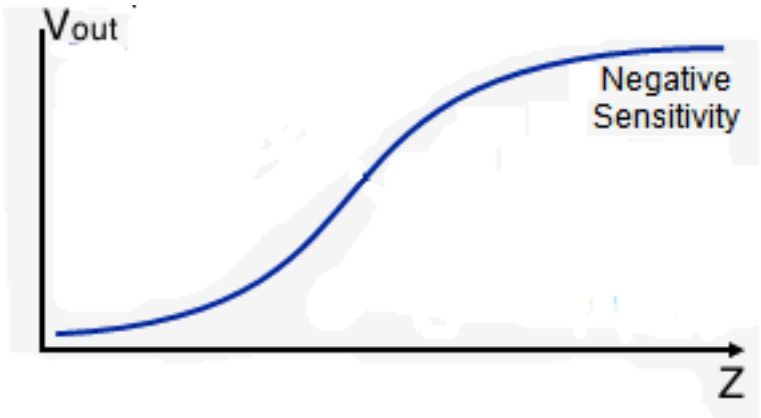

Figure 3.6:Characteristic graph of a hall sensor having a negative sensitivity when a magnet is moved away from the hall sensor.

3.2 INFRARED SENSOR

The Infrared sensor used is an infrared reflective sensor. The reflectivity of the infrared light varies with the colour, texture and distance of the reflecting surface. A LED emits an infrared light, and its reflection by the surface is detected using a phototransistor (see Figure 3.7). The collector current measured depends on the amount of light received on the phototransistor.

To be able to measure relatively big distances, the LED is made to operate beyond its normal operating conditions for a small amount of time so as not to damage the device.

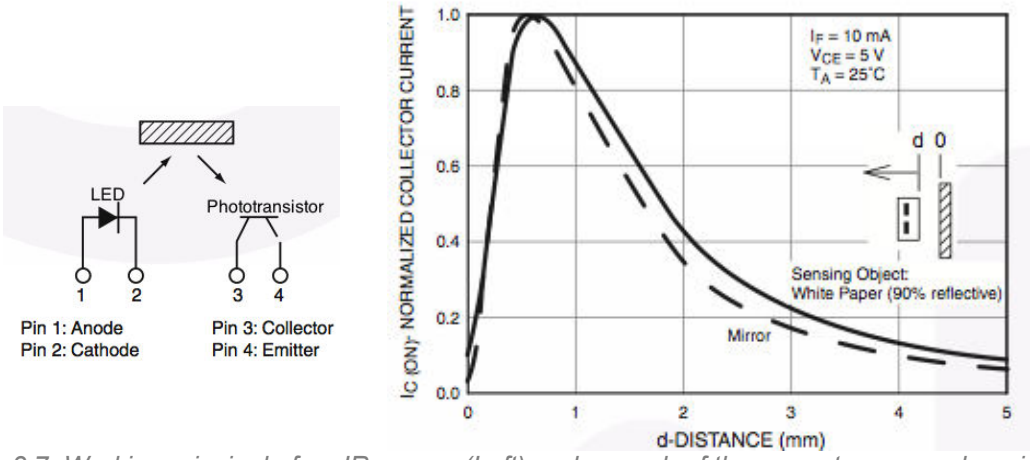

Figure 3.7: Working principal of an IR sensor (Left) and a graph of the current measured against the distance of the object to the sensor (Right) (Ref. 4)

Some problems may arise when using IR sensors. The first one can be observed on the graph above where the sensor gives imprecise measurements if the object is found at less than 0.8mm from it. Another problem is that, the surface of the object may be rotated at an angle that cause the reflected light not to reach the phototransistor (see Figure 3.8)

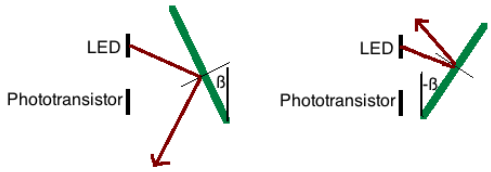

Figure 3.8: Undetectable angular deflection of the surface

4 DETECTABLE GEOMETRIC MISALIGNMENTS

In this section an interest is put on the different geometrical misalignment that can occur when a roombot is engaging docking process with another fix roombot. A theoretical quantitative analysis using both sensors is made to give an indication about the detectable geometrical misalignments and which one can be differentiated from the other. The types of misalignments may be divided into translational, rotational or a combination of both and treated separately.

To undertake this analysis, lets consider a reference placed on the surface of the roombot consisting of x, y, z axes and rotations θ, ϕ, ψ respectively around the axes.

The misalignments are also considered to be small so as displacement remains within the working range of both sensors.

Note that the hall sensors are considered to have a negative sensitivity in the theoretical analysis. Therefore, a hall sensor closer to a magnet will output a lower voltage than a hall sensor further from a magnet.

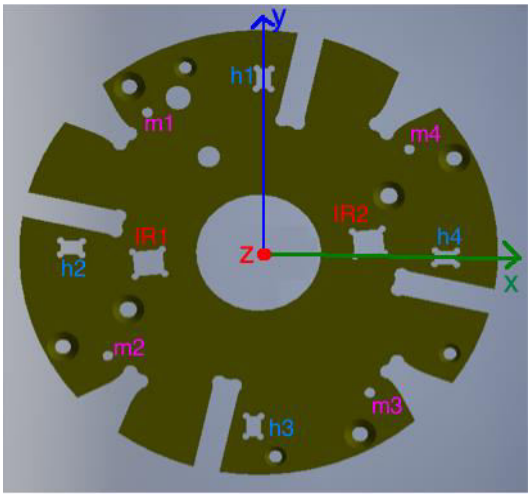

Figure 4.1: Reference placed on roombot's surface

4.1 Translational Misalignment

With purely small translational misalignments the values on the hall sensors will vary by nearly the same amount and there will be no variation on the infrared sensor. Figure 4.2 shows three translational misalignments that can occur.

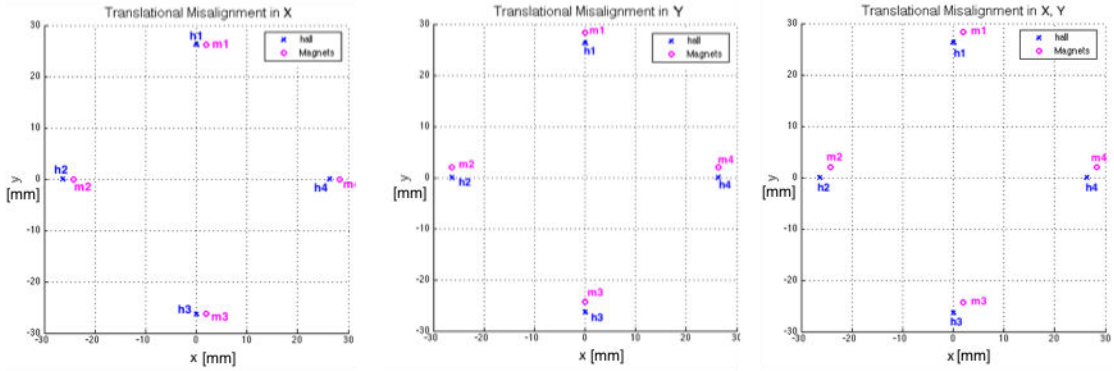

Figure 4.2: Results Of translational misalignments

It has been observed that the distance between the magnets and the hall sensors are the same in each figure and therefore their values will decrease by the same amount. By observing the three graphs from Figure 4.2, it can also be deduced that the hall sensors value will decrease depending on the magnitude of the misalignment but independent on the direction of the misalignment.

4.2 Rotational Misalignment

In this case, pure rotational misalignments were studied between two roombots' surfaces. It can be observed from Figure 4.3 that the three rotational misalignments can be differentiated because the hall sensors will differ depending on the direction and magnitude of the rotation. By observing the values on the hall sensors, on the

left figure, a rotation of $+\Delta\theta$ is detected if hall sensor h3 is smaller than hall sensor h1 and hall sensor h2 equals hall sensor h4.
From the middle figure, a rotation of $+\Delta\phi$ is detected if hall sensor h2 is smaller than hall sensor h4 and hall sensor h1 equals hall sensor h3. From the right figure, a rotation of $+\Delta\psi$ is detected as the four hall sensors measure the same distance and therefore the same value is observed. Note that it is difficult to differentiate between a rotational misalignment of $+\Delta\psi$ and $-\Delta\psi$, and also between a rotational misalignment of $\pm\Delta\psi$ and the three translational misalignments from Figure 4.2 due to the readings on the four hall sensors having the same variation from the aligned position.

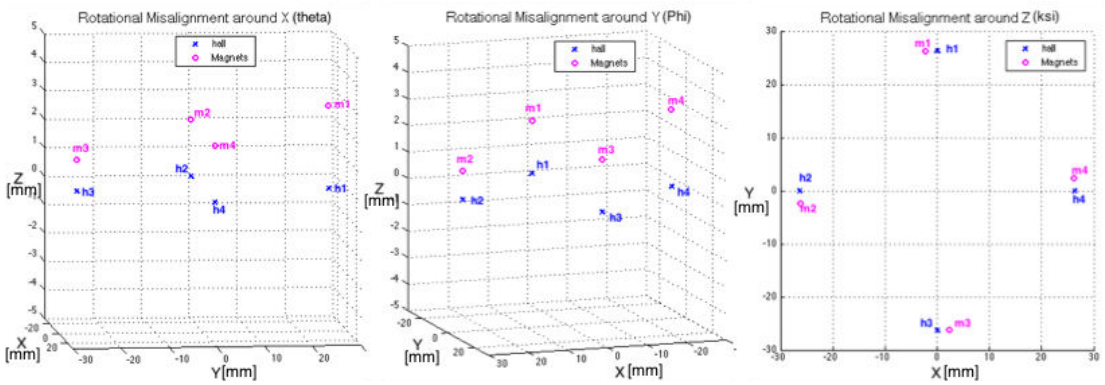

Figure 4.3:Results of rotational Misalignments

The infrared sensor being placed horizontally on the surface of the roombot, it also gives an indication on the rotational misalignment in $\Delta\phi$ only.

Using the readings on the hall sensors only, it is possible to calculate pure angular misalignment in $\Delta\theta$ and $\Delta\phi$.

In $\Delta\theta$:

$$\Delta\theta = \tan^{-1}\left(\frac{d_3 - d_1}{h_{13}}\right)$$

Where, h_{13} is the distance between h1 and h3
d_1 is the distance between magnet m1 and h1
d_3 is the distance between magnet m3 and h3

In $\Delta\phi$:

$$\Delta\phi = tan^{-1}\left(\frac{d_4 - d_2}{h_{24}}\right)$$

Where, h_{24} is the distance between h2 and h4
d_2 is the distance between magnet m2 and h2
d_4 is the distance between magnet m4 and h4

4.3 COMBINATION OF TRANSLATIONAL/ROTATIONAL MISALIGNMENT

In this case it exist a large number of possibilities that has been classified into two groups depending on the readings of both infrared sensors (IR1 and IR2), i.e. if they have the same value or if they differ, and these two groups are divided into subgroups depending on the misalignment that can occur in the two groups. The values on the hall sensors will differ from each other depending on the misalignment in each group. It is difficult using only the hall sensors (without prior knowledge in the state of the moving roombot) to differentiate between the misalignments, between two roombots, that can occur in each group.

4.3.1 Group 1: IR1=IR2

In this case, two combinational misalignments that can occur are:

- *Rotation in ψ, Translation in x and/or y*

  An example is made considering the difference between the hall sensors, h1<h3 and h2>h4. To show that different combinations can yield the same results, by symmetry, on the sensors, two combinational misalignments are done as shown in Figure 4.4

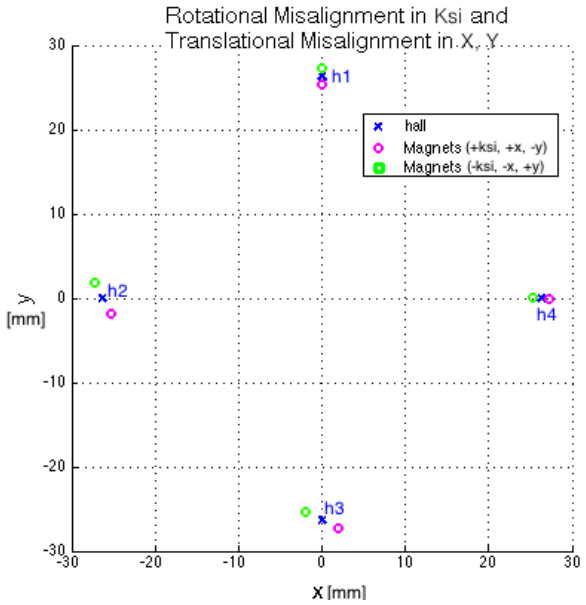

Figure 4.4: Two Combinational Misalignment yielding same results (h1>h3, h2<h4)

It is difficult, in this case, to differentiate between a $+\Delta\psi$ and $-\Delta\psi$ rotational misalignment. The other possible combinations also contain symmetric results, which make them difficult to differentiate.

- *Rotation in θ, Translation in x and/or y*

  In this case, two main differences between the hall sensors are obtained. The first one is h1<h3, h2=h4 and the second one is h1>h3, h2=h4. An example is made considering two different combinations that yield the same results, by symmetry, on the sensors, are shown in Figure 3.5.

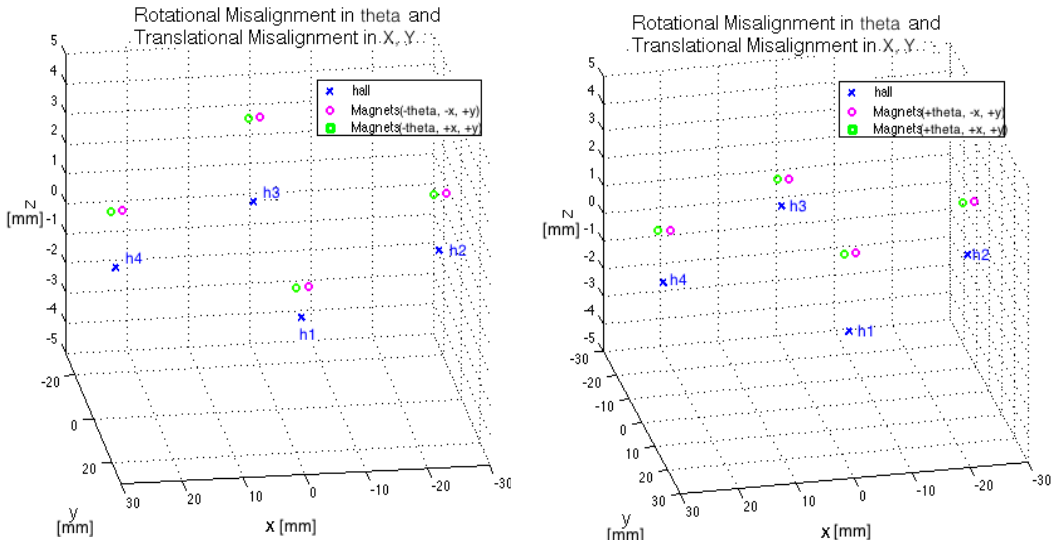

Figure 4.5 : Two combinational misalignments that yield the same results (h1>h3, h2=h4 on the left and h1<h3, h2=h4 on the right)

It is possible, in this case, to detect the sign of a rotational misalignment in $\Delta\theta$. But the translational misalignment cannot be differentiated.

4.3.2 Group 2: IR1≠IR2

In this case, three combinational misalignments that can occur are:

- *Rotation in φ and ψ, Translation in x and/or y*
  Due to the rotation misalignment in φ, the hall sensors values configuration, h2=h4 is not obtained.

- *Rotation in θ and ψ, Translation in x and/or y*
  Due to the rotation misalignment in θ the hall sensors values configuration, h1=h3 is not obtained.

- *Rotation in θ, φ and ψ, Translation in x and/or y*
  Due to the rotation misalignment in θ and φ, the hall sensors values configuration, h1=h3 and h2=h4 are not obtained.

In the three subgroups above it is difficult, using both sensors, to differentiate in each case and between each case the combined misalignment between two roombots. To conclude this section, with both the infrared sensors and the hall sensors used alone; it is difficult to differentiate between all the possible misalignments.

5 EXPERIMENTS TO TEST AND CHOSE THE SENSORS

In this section, a characterisation of different hall sensors having different negative sensibility and a characterisation of the infrared sensor has been done.

5.1 THE SETUP

To be able to characterize the different mode of motion of the hall sensors and choose the best hall sensor that suits best the application, a test setup has been mounted. The characteristics of the infrared sensors were also quantitatively obtained with this setup.

The setup consists of a lathe that provides precise z and lateral movement (R) (see Figure 4.1). Supports have been designed to fixed one roombot face on the circular clutch of the lathe and the other roombot face, facing the first one, on the chisel holder of the lathe.

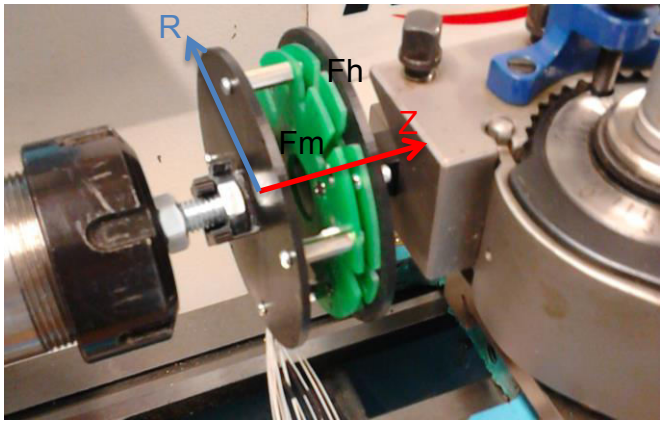

Figure 5.1:Mounted Roombot faces on setup

5.2 HALL SENSOR TESTS

5.2.1 Method

To obtain the characteristic in head on and lateral motion, the roombot face (Fh) with the hall sensors mounted was moved away in Z from the roombot face (Fm) mounted with the magnets. Then at a fixed Z distance, Fh is made to move in lateral direction (+R). A symmetric hypothesis has been made, as the magnetic field around the magnet is symmetric. The face Fh is moved by a small distance ΔR, if the digital output of the hall sensor varies a lot. Therefore fine measurement is done in the detectable region of the hall sensor. This is repeated for 5 different values of Z. Appendix A shows a table of the data collected for two different values of Z.

4 hall sensors and 3 magnets having different diameters have been tested. See Table 5.1.

Table 5.1:Hall sensors and magnets that have been tested (Ref. 8)

Magnet diameter [mm]	Hall sensor Sensitivity
2	DVR5053OA (-11mv/T)
3	DVR5053PA (-23mv/T)
4	DVR5053RA (-45mv/T)
-	DVR5053VA (-90mv/T)

Every combination of hall-magnet pair in head on and slide by movement configuration has been tested in order to choose the suitable pair. The choosing criteria are:

- A small saturation region
- A large detectable region
- A smooth transition in the detectable region

The problem of having a small saturation region is the decrease in the detectable region. Therefore, a trade off between a small saturation region and a large detectable region need to be found. A smooth transition region is needed so as the roombot does move directly from the saturation region to the undetectable region or vice versa when it does a small displacement.

5.2.2 Results

In the results obtained, a comparison between the different saturation, detectable and transition area has been done. The result is given in Table 5.2.

Table 5.2: Comparison table of the different region of the Hall-Magnet pair

Hall	Magnets [mm]	Saturation Area [mm^2]	Detectable Area [mm^2]	TransitionDistZ [mm]	TransitionDistR [mm]
OA	2	0.15	8.59	2.25	1.16
	3	0.43	14.60	2.76	1.62
	4	1.86	26.57	2.00	2.16
PA	2	1.53	15.51	2.32	1.50
	3	2.87	15.37	2.88	1.50
	4	3.23	27.01	2.89	1.34
RA	2	3.39	21.76	2.16	1.56
	3	5.97	31.19	2.20	1.56
	4	11.56	31.51	3.30	1.88
VA	2	7.50	17.34	2.40	1.88
	3	13.57	40.47	4.14	2.5
	4	31.07	56.04	3.78	1.58

From the table above, the trend that can be observed is that a large magnet diameter or a high sensitivity hall magnet increases both the saturation area and the detectable area. The transition in z (head on) and R (radial) is generally less steep with an increase in the diameter of the magnet.

Using the choice criteria described in the previous section, the hall sensor VA has been directly eliminated due to the high saturation area. The hall sensor OA with a 4mm magnet, PA with 2mm magnet and RA with a 3mm magnet have been chosen as the best candidates for the application. Figure 5.2 shows the characteristics of the chosen hall sensors. The data obtained during testing was used to make 3D fit so as to characterise the hall sensor in z and R direction in one graph. A contour plot has been done so as to be able to differentiate the different regions of interests.

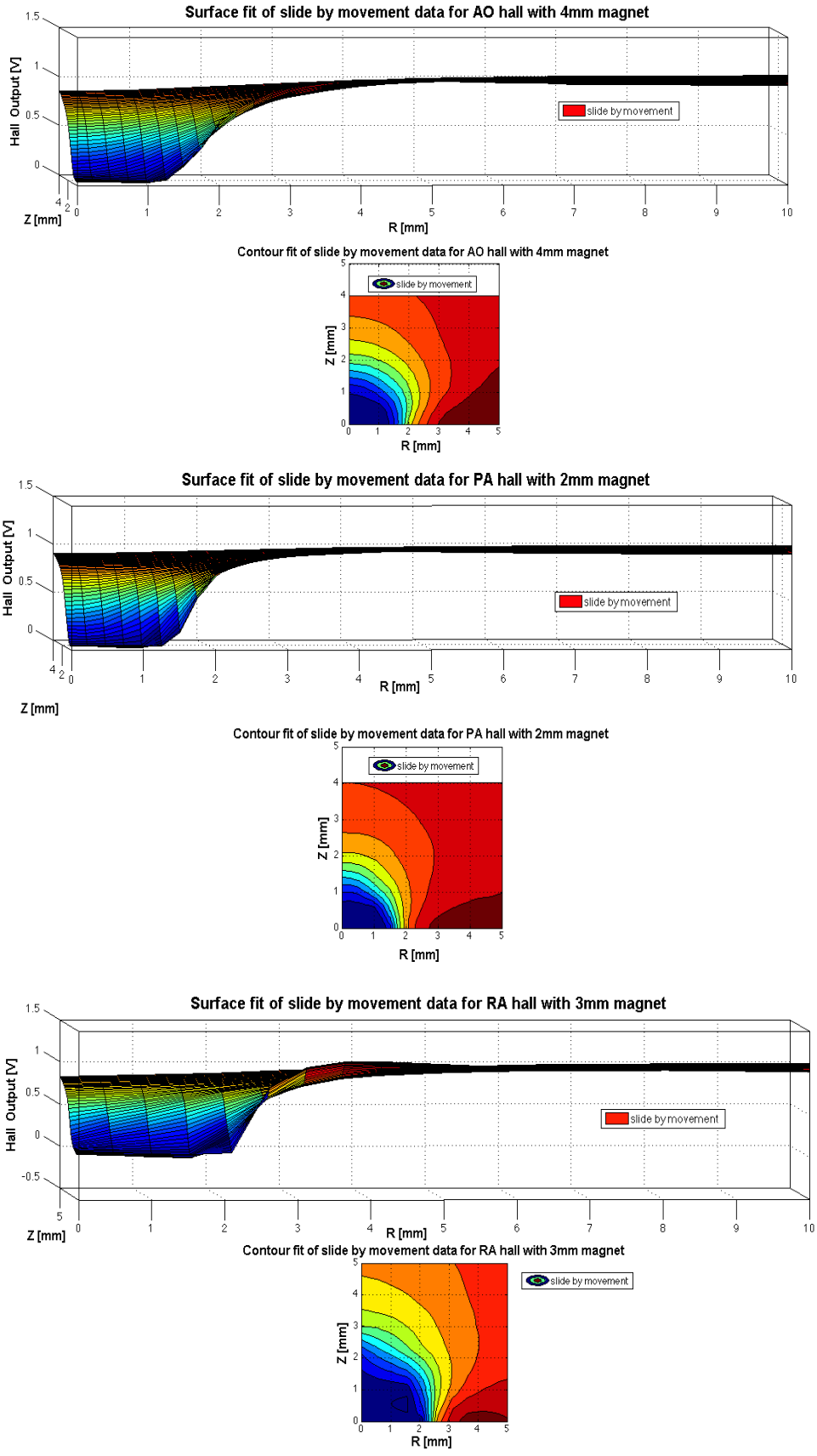

Figure 5.2: From top to bottom: characteristic of the hall sensors chosen. In dark blue is the saturation zone and the detectable zone is found between the dark blue zone and the red zone.

Table 5.3 : Operating Range in Z and R obtained from the previous graphs

Chosen Sensor Magnet Pair	Range in Z [mm]	Range in R [mm]
AO hall 4mm magnet	1 - 4	1.25 – 3
PA hall 2mm magnet	1 - 4	1.25 – 3.5
RA hall 3mm magnet	1 - 5	1.25 - 3

From Figure 5.2, it can be observed that the saturation region in dark blue for the OA hall with a 4mm magnet and the PA with 2mm magnet stays within 1mm in head on (Z) and lateral (R) direction whereas the RA hall has higher saturation region due mainly to its higher sensitivity. But the detectable region is higher for the RA compared to the two other combination considered. It can be noticed also that a small overshoot starts to appear as the sensitivity of the hall sensor increases (see Appendix A.2 too observe this phenomenon on the VA hall sensor which has a higher sensitivity). This overshoot may be due to the sensor sensing the magnetic lines coming from the north pole of the magnet.

Further testing need to be undergone in this case directly on the roombot with these sensors mounted so as to characterise their behaviour in a real situation. What needs to be considered also are the movement resolution of the roombot and the tolerance in the alignment. For example, if the tolerance in the alignment is out of the saturation region, the roombot can be operated in on and off mode, i.e. if the sensors saturates then it is aligned and it is misaligned otherwise. If the tolerance is within the saturation region, the alignment will not be possible. Concerning the resolution of the roombot, a too high resolution may cause the roombot to get difficulty to stay in the detectable region of the hall sensors, making alignment difficult. The difficulty increases if the tolerance is much smaller than the saturation region.

5.3 Infrared Sensor Tests

A characterisation of the infrared sensors mounted on the roombot is done for the green, mate roombot's face and also for different orientations.

5.3.1 Method

For the first experiment, the roombot faces were placed parallel to each other. The faces were moved away from each other in the z direction and the data obtained from both mounted infrared sensors were recorded.
For the second experiment the roombot faces were placed at different angles, in θ and ϕ, to each other. Then the faces were made to move away from each other in z direction. (See Figure 5.3)

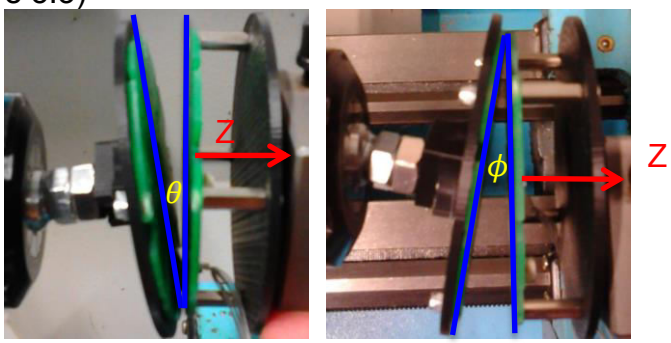

Figure 5.3: Roombots faces in $\theta$and ϕ misalignment

5.3.2 Results

The data collected were plotted for the different configurations.

Parallel Faces in z movement

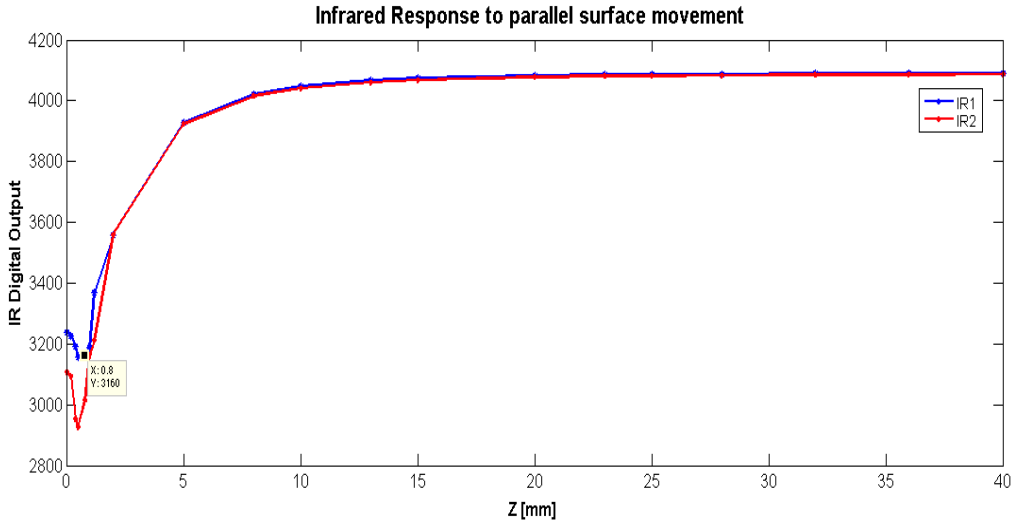

Figure 5.4:Infrared response in parallel motion

In Figure 5.4 it can be observed that the infrared sensor is not precise below a 0.8mm distance between the two roombot's faces. In parallel motion it can be concluded that the infrared sensors can be used within a range of 0.8 to 10mm. Compared to datasheet of the infrared sensor, the maximum detectable distance is almost doubled. This is due to the led being supplied with a large amount of current for a short period of time, increasing the intensity of the IR beam emitted. It can also be observed that both sensors are consistent when the surfaces are parallel.

ϕ Misaligned Faces in z movement

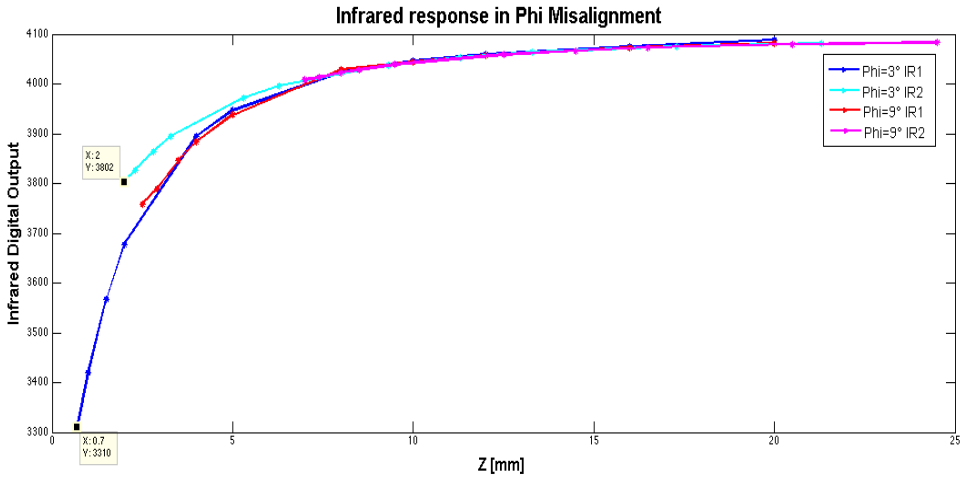

Figure 5.5:Phi misalignment detected by infrared sensor

From Figure 5.5, it can be observed that a rotational misalignment greater than 9° is not detectable by the infrared sensors as IR2 detect anything from this point.

Considering Figure 5.6, trigonometric formulas can be obtained to calculate the misalignment in ϕ.

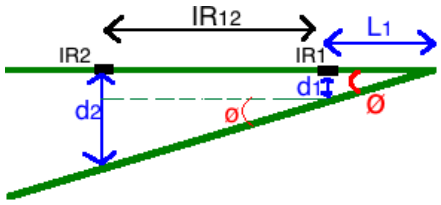

Figure 5.6: ϕ Calculation: Graphical representation

The smallest ϕ angle measurable can be calculated knowing the minimum measurable distance of 0.8mm and introducing it in the following formula:

$$\phi = \tan^{-1}\left(\frac{d_1}{L_1}\right) = \tan^{-1}\left(\frac{0.8}{17.20}\right) = 2.7°$$

In the detectable range, by comparing IR1 with IR2, it is possible to calculate the angular misalignment ϕ with the following formula:

$$\Delta\phi = tan^{-1}\left(\frac{d_2 - d_1}{IR_{12}}\right)$$

Where, IR_{12} is the distance between IR1 and IR2
d_1 is the distance between IR1 and roombot's surface
d_2 is the distance between IR2 and roombot's surface

θ Misaligned Faces in z movement

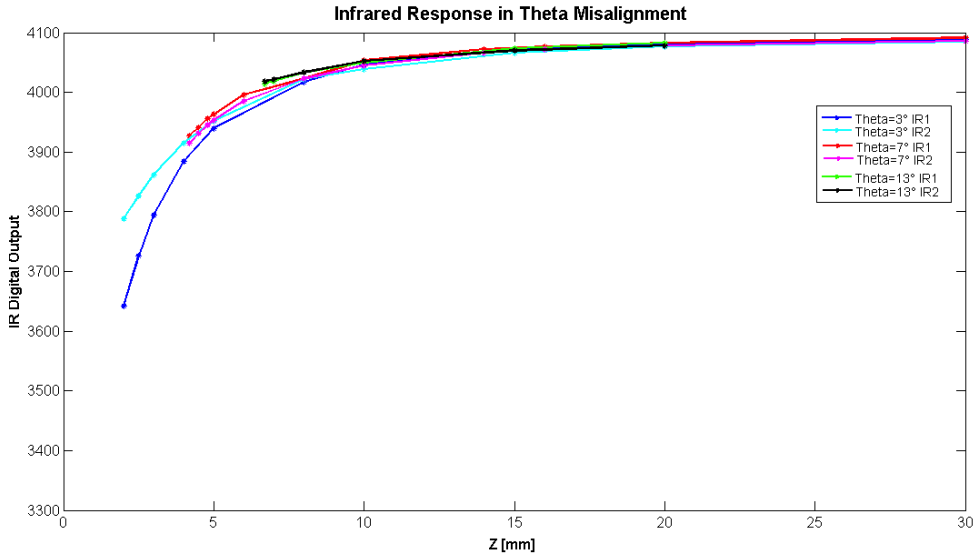

Figure 5.7: Infrared sensor response to Theta Misalignment

From Figure 5.7, it is difficult to obtain the misalignment in θ because both infrared sensors give almost the same output as they have the same distance from the surface in front.

6 TESTS ON ROOMBOT HARDWARE

6.1 A REGION OF INTEREST INSIDE THE WORKSPACE TO PERFORM ALIGNMENT TESTS ON THE ROOMBOT

To find a region were the roombot metamodule could move without any degrees of freedom blocked and inverse kinematic solvable, Webots simulation environment was used. At first forward kinematics was used to define the joint coordinates so as the roombot metamodule is placed in a desired configuration in space. But when switching to inverse kinematics, in a goal to test if the roombot can move freely from the initial configuration, the algorithm compute another solution and the initial desired joint configuration is changed. It is therefore difficult to initialise the roombot with a desired joint angle configuration using forward kinematics.
A more iterative approach was used using directly inverse kinematics so as to bring the robot into a desired configuration. The result obtained is shown in Figure 6.1. Note that the roombot was first initialised at x=100mm, y=0mm, z=270mm, tx=90°, ty=90° and tz=0°.

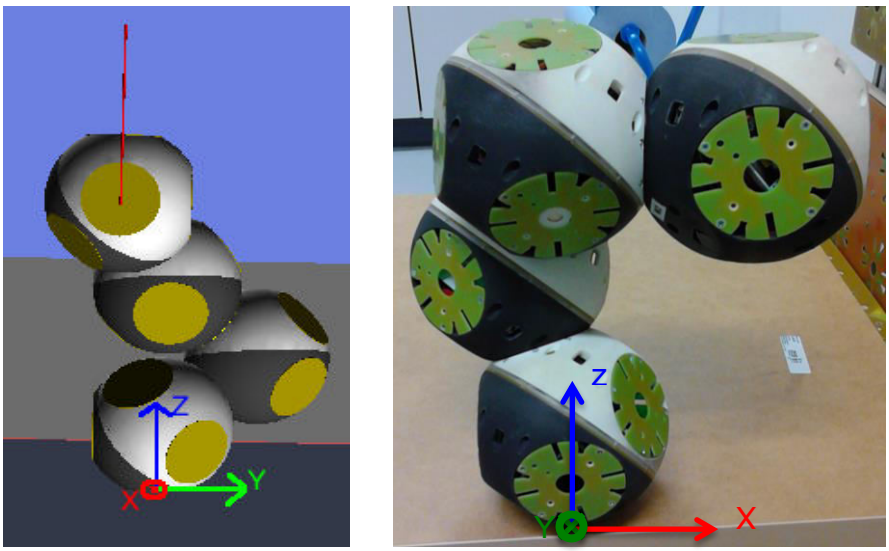

Figure 6.1: Webots Configuration (left) and Real configuration (Right)

This configuration was chosen because the forces acting on the roombot are balanced making it stay in an equilibrium position without any support. This configuration also enables a good range of movement for its six degrees of freedom end effector.
Table 6.1 shows the different joint and end effector coordinates for the configuration in Figure 6.1. The range of motion in the end effector coordinates is also given.

Table 6.1: End effector coordinate, joint coordinates and its movable range

x [mm]	Δx [mm]	y [mm]	Δy [mm]	z [mm]	Δz [mm]	tx [°]	Δtx [°]	ty [°]	Δty [°]	tz [°]	Δtz [°]
128	-168;+121	-26	-161;+146	289	-40;+47	90	±20	90	±20	0	±30
q1		**q2**		**q3**		**q4**		**q5**		**q6**	
-59.4		-103		-128		20.5		-103		71.8	

To test close docking approach using the sensors mounted on the faces, the configuration in Figure 6.1 enables the movement of the end effector within a quite large range.

Due to the reading of the sensor values send by the roombot to PC not implemented, the testing using inverse kinematic with the above configuration was not done. Instead, CuteCom was used to test the behaviour of the sensors by receiving the sensor data and setting the motor angle considering the configuration in Figure 6.2. The tests were done with the AO hall sensor mounted together with the 3mm and 4mm magnet (See Table 6.2 and Table 6.3). Another test was done with the RA hall sensor with the 3mm magnets mounted. (See Table 6.4).

Figure 6.2: On the Right figure: testing configuration with mounted sensors on the roombot on the left and the magnets mounted on the roombot on the right. On the Left figure, the angular misalignment resulting from a rotation motor 1 by 3°

Due to loose gear of the ACM causing the slipping of the motor, it was difficult to close firmly the grippers. So to test if it docks or not, the grippers entering the female opening was tested. The translation R is set so as the ACM are not aligned to the female opening to see if the hall sensors indicates a misalignment.

Table 6.2: Result obtained with AO hall and 4mm magnet

	Hall 1	Hall 2	Hall 3	Hall 4	IR1	IR2	Docking
Z=0	68	52	44	54	3352	3526	YES
Z=0, R	1291	1281	1304	1293	2582	3034	NO
Z=3mm	1009	899	953	1009	3575	3858	YES
Motor1=3°	929	567	261	804	3356	3599	NO

Table 6.3: Result obtained with AO hall and 3mm magnet

	Hall 1	Hall 2	Hall 3	Hall 4	IR1	IR2	Docking
Z=0	65	57	46	52	3912	3030	YES
Z=0, R	1267	1281	1294	1274	3259	2970	NO
Z=3mm	1102	1000	1069	1110	3799	3703	YES
Motor1=3°	1154	1003	853	1119	3643	3350	NO

In translation, the OA hall sensors are able to detect an unsafe docking (undetectable zone) when the roombots are misaligned and a safe docking when aligned (Saturation zone).

When the motor 1 is turned by 3° the corresponding magnet will be in theory closer to h2 and h3 detecting a combined misalignment in ϕ and θ (h2 < h4 and h3 < h1 respectively). This is observed with OA hall and 4mm magnets. With the 3mm magnet the difference is less significant as the graph (See Appendix A) flattens sooner and therefore it becomes more difficult to detect the resulting rotational misalignment.

Table 6.4: Result obtained with RA hall and 3mm magnet

	Hall 1	Hall 2	Hall 3	Hall 4	IR1	IR2	Docking
Z=0	66	48	48	50	3560	4095	YES
Z=0, R	1152	1147	1095	1220	3380	4095	NO
Z=3mm	888	855	756	975	3899	4095	YES
Motor1=3°	1160	1277	133	1100	3694	4095	NO

Note that IR2 is not working properly as it always return 4095. This may be due o a connection problem.
In translation, the RA hall sensors are also able to detect an unsafe docking when the roombots are misaligned and a safe docking when aligned.

7 CONCLUSION

Firstly, a theoretical analysis of the different misalignments has been done. It was observed that the mounted hall sensors and infrared sensors alone couldn't be used to detect a specific misalignment. This is due to the number of symmetrical solutions obtained. One reason of this is that the hall sensor measures only an absolute distance. The infrared sensors give an indication of the parallelism and therefore help to eliminate some solutions. By combining these sensory feedback to the input commands sent to the motor, the misalignment can be known.

Then, the sensors have been characterized especially the different hall sensors so as to choose the bests hall sensor magnet pair. For this purpose, a test setup has been mounted and data collected for the hall sensor in head on and slide by motion, and for the infrared sensor, in parallel motion, in ϕ misalignment and in θ misalignment.

To do further testing of the sensors and to evaluate the close docking process using local sensory feedback, the sensors and new ACM has been mounted on a roombot metamodule. A region where the roombot can move freely has also been identified in its workspace using Webot.

Some test on the real hardware has been performed showing that the sensors gives an indication on if it is safe to dock or not. Further tests needs to be performed on the sensors during a real situation.

7.1 ACKNOWLEDGMENT

I would like to thank Mehmet Mutlu for his support, availability and in giving me the opportunity to learn and practice SMD soldering, and to play with the roombot during this semester project.
I also would like to thank Professor Auke Ijspeert for welcoming me in the laboratory and giving me the opportunity to work on this interesting project.

Appendix A

A.1 Sample of Data collected in slide by movement tests for PA hall sensor with 2mm magnet.

TableA.1: Example of Data sample collected

Z [mm]	R [mm]	Hall	Hall	Hall	Hall	Hall	Hall Mean	Z [mm]	R [mm]	Hall	Hall	Hall	Hall	Hall	Hall Mean
0	0	49	49	49	49	49	49	0.5	0	51	51	51	51	51	51
0	0.2	49	49	49	49	49	49	0.5	0.2	51	51	51	51	51	51
0	0.4	50	50	50	50	50	50	0.5	0.4	51	52	51	51	52	51
0	0.8	50	50	50	50	50	50	0.5	0.8	53	53	53	53	53	53
0	1	51	51	51	51	51	51	0.5	1	56	56	56	56	56	56
0	1.2	53	53	53	53	53	53	0.5	1.2	205	206	206	207	206	206
0	1.4	84	85	86	86	85	85	0.5	1.4	407	408	406	408	406	407
0	1.8	750	749	747	748	748	748	0.5	1.8	807	808	807	806	807	807
0	2	954	951	953	954	951	953	0.5	2	931	932	934	935	931	933
0	2.3	1125	1126	1128	1126	1125	1126	0.5	2.3	1064	1063	1062	1064	1063	1063
0	2.6	1217	1219	1221	1225	1226	1222	0.5	2.6	1158	1157	1159	1158	1159	1158
0	3	1273	1274	1276	1275	1278	1275	0.5	3	1217	1217	1218	1217	1214	1217
0	3.2	1285	1286	1284	1284	1285	1285	0.5	3.2	1236	1232	1232	1232	1234	1233
0	3.4	1310	1308	1309	1308	1310	1309	0.5	3.4	1245	1244	1244	1242	1243	1244
0	3.6	1308	1307	1309	1308	1308	1308	0.5	3.6	1251	1253	1251	1252	1251	1252
0	4	1303	1304	1303	1303	1305	1304	0.5	4	1257	1258	1259	1260	1257	1258
0	4.2	1298	1298	1300	1300	1299	1299	0.5	4.2	1257	1260	1259	1258	1259	1259
0	4.4	1297	1297	1296	1297	1297	1297	0.5	4.4	1259	1258	1259	1260	1258	1259
0	4.8	1273	1271	1270	1273	1271	1272	0.5	4.8	1256	1255	1256	1257	1255	1256
0	5	1264	1267	1264	1266	1266	1265	0.5	5	1256	1256	1257	1252	1255	1255
0	5.5	1258	1262	1261	1260	1258	1260	0.5	5.5	1249	1249	1248	1250	1249	1249
0	6	1252	1254	1252	1255	1254	1253	0.5	6	1246	1247	1247	1248	1244	1246
0	6.5	1248	1247	1250	1248	1247	1248	0.5	6.5	1243	1244	1243	1245	1242	1243
0	7	1244	1243	1245	1244	1243	1244	0.5	7	1241	1238	1239	1240	1239	1239
0	8	1236	1239	1240	1242	1237	1239	0.5	8	1236	1238	1237	1233	1235	1236
0	9	1232	1237	1234	1238	1237	1236	0.5	9	1233	1231	1231	1232	1233	1232
0	10	1231	1233	1232	1231	1234	1232	0.5	10	1229	1229	1230	1231	1232	1230
0	11	1229	1230	1231	1229	1230	1230	0.5	11	1229	1228	1228	1229	1228	1228
0	11.5	1230	1231	1229	1228	1230	1230	0.5	11.5	1228	1229	1229	1228	1228	1229
0	12	1228	1229	1231	1230	1230	1230	0.5	12	1229	1228	1227	1229	1228	1228

Table A.1 shows the type of data collected from the hall sensors that has been used to evaluate their characteristics with a certain magnet size. Several measurements were done and the mean of the digital output of the hall sensors calculated. This was done for several z (head on distance between the hall sensor and the magnet). In Table A.1, only two z distances is shown, but this was repeated for several z distances and for every hall magnet pair possible. To convert the data in volts the following formula was used:

$$\textbf{hall output } [\mathbf{V}] = \textbf{hall Mean} * \frac{\mathbf{3.3\ [V]}}{\mathbf{2^{12} - 1}}$$

The value 12 correspond to the 12 bit analogue to digital convertor (ADC)

A.2 Other Hall sensor plots obtained

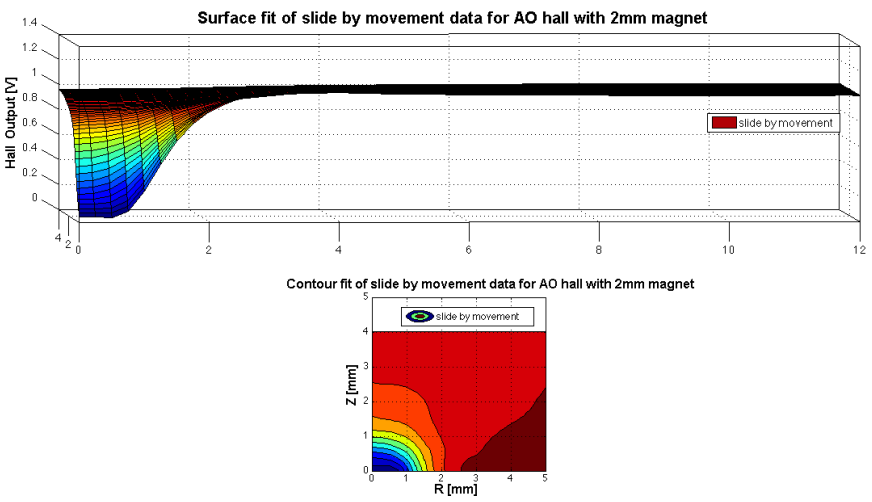

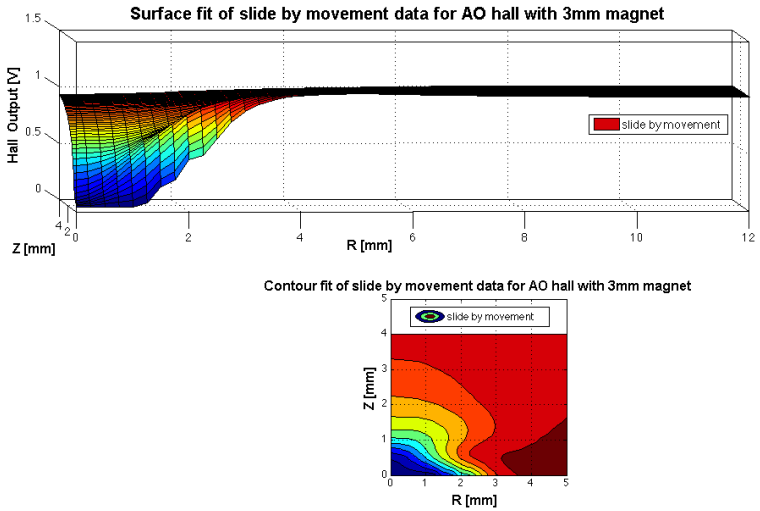

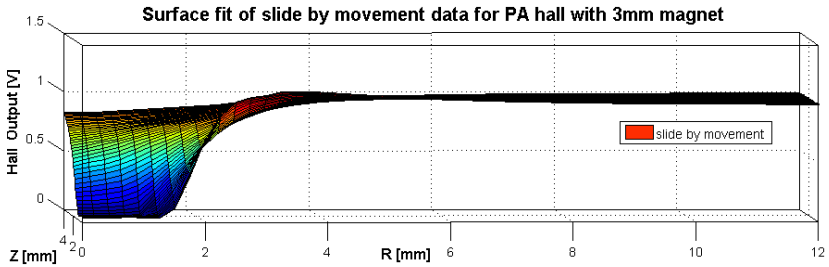
Surface fit of slide by movement data for PA hall with 3mm magnet
Hall Output [V]
slide by movement
Z [mm]
R [mm]

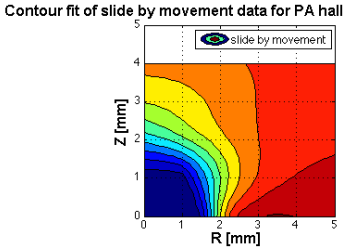
Contour fit of slide by movement data for PA hall with 3mm magnet
slide by movement
Z [mm]
R [mm]

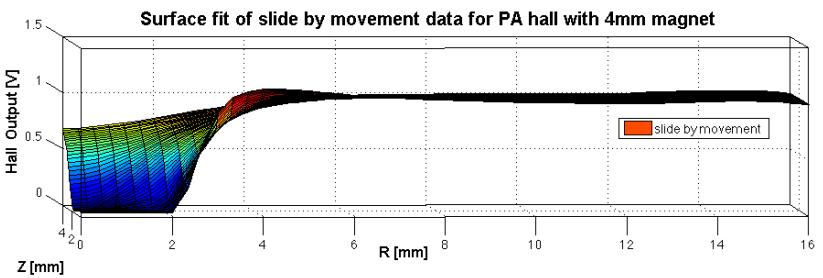
Surface fit of slide by movement data for PA hall with 4mm magnet
Hall Output [V]
slide by movement
Z [mm]
R [mm]

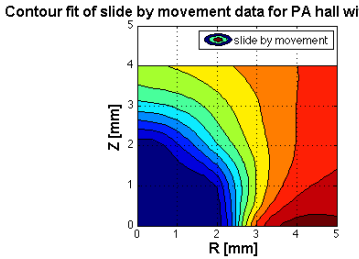
Contour fit of slide by movement data for PA hall with 4mm magnet
slide by movement
Z [mm]
R [mm]

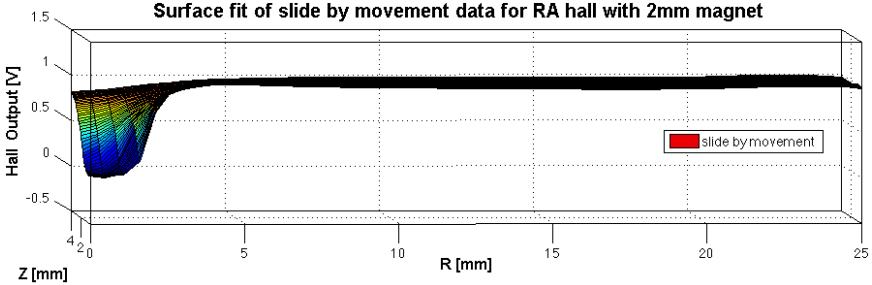
Surface fit of slide by movement data for RA hall with 2mm magnet
Hall Output [V]
slide by movement
Z [mm]
R [mm]

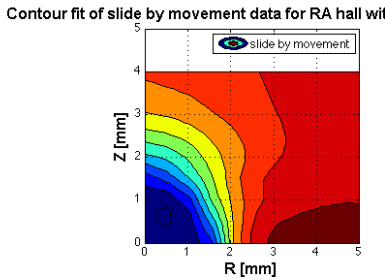
Contour fit of slide by movement data for RA hall with 2mm magnet
slide by movement
Z [mm]
R [mm]

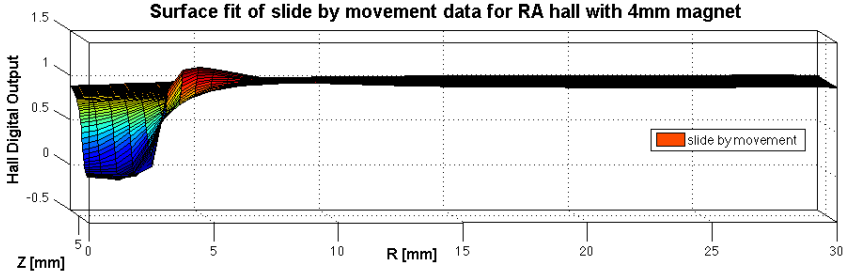
Surface fit of slide by movement data for RA hall with 4mm magnet
Hall Digital Output
slide by movement
Z [mm]
R [mm]

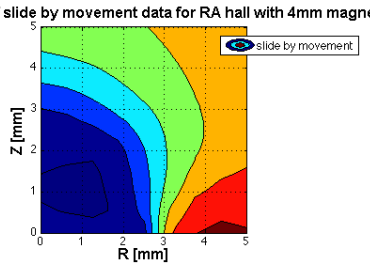
Contour fit of slide by movement data for RA hall with 4mm magnet
slide by movement
Z [mm]
R [mm]

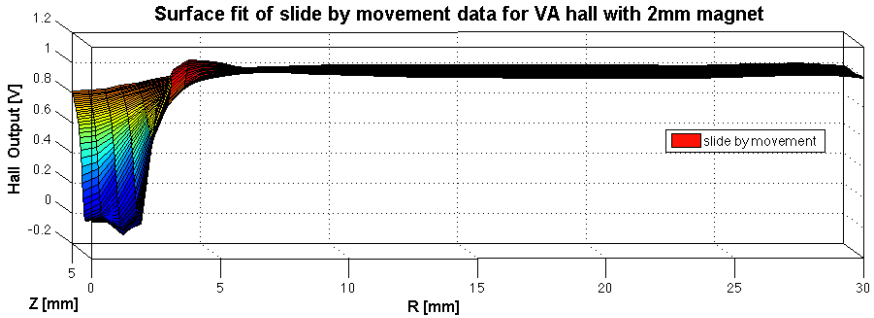
Surface fit of slide by movement data for VA hall with 2mm magnet
Hall Output [V]
Z [mm]
R [mm]
slide by movement

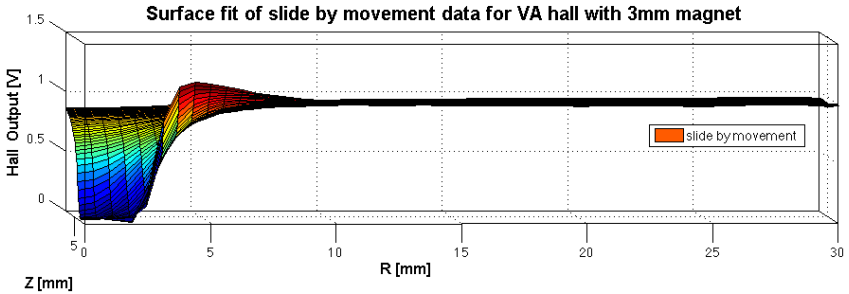
Surface fit of slide by movement data for VA hall with 3mm magnet
Hall Output [V]
Z [mm]
R [mm]
slide by movement

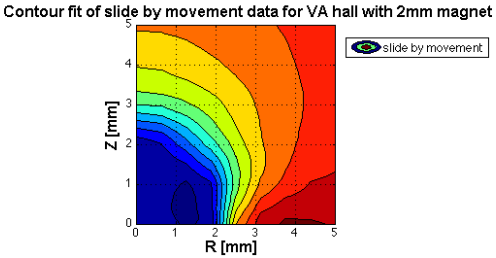
Contour fit of slide by movement data for VA hall with 2mm magnet
Z [mm]
R [mm]
slide by movement

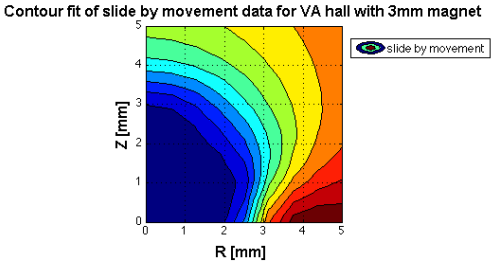
Contour fit of slide by movement data for VA hall with 3mm magnet
Z [mm]
R [mm]
slide by movement

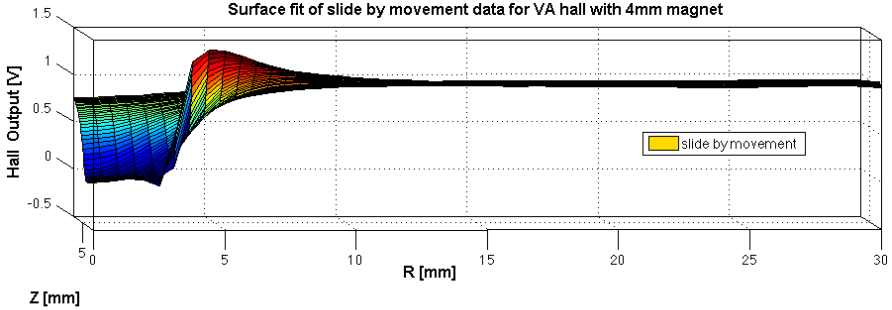
Surface fit of slide by movement data for VA hall with 4mm magnet
Hall Output [V]
Z [mm]
R [mm]
slide by movement

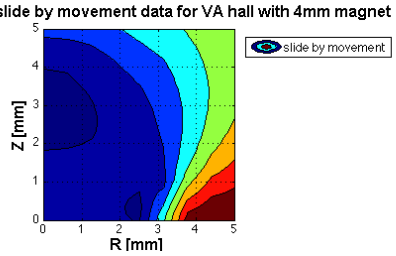
Contour fit of slide by movement data for VA hall with 4mm magnet
Z [mm]
R [mm]
slide by movement

8 REFERENCES:

1. A. Spröwitz, R. M. (2013). Roombots: A hardware perspective on 3D self-reconfiguration and locomotion with a homogeneous modular robot. *Robotics and Autonomous Systems* .

2. Alexander Spröwitz, S. P. (2010). Roombots: Reconfigurable Robot for Adaptive Furniture. *IEEE COMPUTATIONAL INTELLIGENCE MAGAZINE* .

3. Allegro MicroSystems, L. (n.d.). Hall-Effect IC Applications Guide. Worcester, Massachusetts , USA: Allegro MicroSystems, LLC.

4. Corporation, F. S. (2009, September). QRE1113, QRE1113GR Minature Reflective Object Sensor.

5. Hossein Ahmadzadeh, E. M. (2015). Modular Robotic Systems: Characteristics and Applications. *Journal of Intelligent and Robotic Systems* .

6. Hossein Ahmadzadeh, E. M. (2015). Modular robotic systems: Methods and algorithms for abstraction, planning, control, and synchronization. *Artificial Intelligence* , 27-64.

7. Inc, h. (n.d.). HALL EFFECT SENSING AND APPLICATION. Illinois, USA.

8. Incorporated, T. I. (2015, December). DRV5053 Analog-Bipolar Hall Effect Sensor Datasheet. Texas, USA.

9. Incorporated, T. I. (n.d.). *Texa Instruments Sensing Solutions*. Retrieved April 25, 2016 from http://www.ti.com/lsds/ti/analog/sensors/what-are-you-sensing.page#proximity

10. Yanhe Zhu1, H. J. (2014). A Multi-sensory Autonomous Docking Approach for a Self-reconfigurable Robot without Mechanical Guidance. *International Journal of Advanced Robotic Systems* .